Solid State Phenomena
ISSN: 1662-9779, Vol. 390, pp 197-205
doi:10.4028/p-AoUE30

Submitted: 2026-01-21
Revised: 2026-02-25
Accepted: 2026-02-25
Online: 2026-04-17

A Compact Micromechanical Model for the Elastic-Viscoplastic Deformability of PLA-Hemp Biocomposites

NIANG Ndeye[1,a], HOLOPAINEN Sami[2,b], BARRIERE Thierry[1,c*], PLACET Vincent[1,d] and GABRION Xavier[1,e]

[1]Marie and Louis Pasteur University, SUPMICROTECH-ENSMM, CNRS, Institute FEMTO-ST, F-25000 Besancon, France

[2]Tampere University, Department of Civil Engineering, FI-33014 Tampere, Finland

[a]ndeye.niang@femto-st.fr , [b]sami.holopainen@tuni.fi , [c *]thierry.barriere@univ-fcomte.fr, [d]vincent.placet@umlp.fr , [e]xavier.gabrion@univ-fcomte.fr

Keywords: Biocomposite, Viscoplasticity, Machine learning, 3D-printing, Forming

Abstract. Despite the growing use of biopolymers in automotive, packaging and structural applications, predictive modelling of their elastic–viscoplastic deformation remains limited. In this work, a micromechanically based constitutive model is proposed to describe the micro-to-macroscopic behaviour of a semi-crystalline PLA matrix reinforced with short hemp fibers. The formulation relies on a multiplicative split of the deformation gradient into elastic and viscoelastic–plastic parts, with elasticity governed by fiber and crystalline phases and time-dependent deformation localized in the amorphous phase. High fiber content and strong fiber–matrix bonding enable the suppression of lattice crystalline anisotropy, leading to a compact model with a reduced number of internal variables. The model is calibrated and validated using uniaxial tensile tests on pellet-extrusion 3D-printed specimens with controlled porosity and plasticiser content, and reproduces nonlinear loading, unloading, creep and stress relaxation. In a second step, synthetic data generated by the constitutive model are used to train surrogate machine-learning models, which are discussed as a perspective for accelerating long-term simulations and parametric studies in forming applications.

Introduction

Natural short-fiber reinforced (NSFR) polymer composites represent a promising class of sustainable materials that reduce dependence on petroleum-derived plastics across forming-intensive applications, including automotive structures, packaging, and biomedical devices [1]. Polylactic acid (PLA) matrices reinforced with plant fibers such as hemp offer tunable mechanical properties through systematic variation of fiber content, matrix crystallinity, and processing-induced porosity. However, the inherent viscoelastic-plastic deformation characteristics of these materials manifested through time-dependent creep, strain rate sensitivity, and irrecoverable residual strains present significant challenges for reliable process simulation and design optimisation. Traditional experimental characterisation proves both costly and time-intensive, particularly when exploring expansive parameter spaces involving multiple fiber types, plasticiser formulations, and manufacturing conditions.

Previous modelling efforts for short-fiber biocomposites have mainly relied on mean-field homogenization or full-field finite element analyses of idealized microstructures. Orientation-averaging approaches for natural fiber composites capture stiffness reasonably well but remain computationally expensive and poorly adapted to large viscoplastic strains [2–4]. Mean-field schemes for randomly distributed short fibers also require complex fitting to link micro-scale parameters to macroscopic behaviour. In contrast, phenomenological viscoelastic or viscoplastic laws are computationally efficient but often disconnected from microstructural quantities such as fiber content, degree of crystallinity and porosity.

In this work, a compact micromechanical constitutive model is developed for PLA–hemp biocomposites that bridges micro- and macro-scales while remaining numerically efficient [1]. The

key idea is to exploit the high stiffness of the short hemp fibers and their strong bonding to the semi-crystalline matrix to suppress explicit lattice-scale anisotropy, and to represent the fibers and crystalline phase by Hencky-type elastic laws while concentrating viscoelastic–plastic flow in the amorphous phase. The model is calibrated from a limited experimental dataset and validated under uniaxial tension, including creep and relaxation. As a perspective, the model is then used as a physics-based data generator to train machine-learning surrogates for rapid, long-term predictions.

Materials Processing and Experimental Characterisation

Materials Processing

Commercial PLA (PLI 005 grade, Natureplast) served as the matrix material, compounded with short hemp fibers (average length 160 µm, obtained through hammer milling and defibration) at 20 wt% loading and polyethylene glycol plasticizer at 5 wt% respectively PEG 1500 and PEG 20000. Twin-screw extrusion processing occurred at 190°C and 30 rpm rotation speed to ensure homogeneous dispersion while minimizing thermal degradation. The resulting pellets underwent drying treatment (60°C for 3 hours) prior to P-MEX 3D-printing of ISO 527-4 Type 1B dogbone tensile specimens as shown in Fig.1. Optimised printing parameters included nozzle temperature of 190°C, layer thickness of 0.4 mm, and print speed of 40 mm/s, balancing extrudability, surface quality, and microstructural development. These conditions produced controlled porosity levels of 8-9% that proved essential for achieving ductile deformation behavior at ambient temperature, overcoming the inherent brittleness of pure PLA (ultimate strain <1%) [5,6].

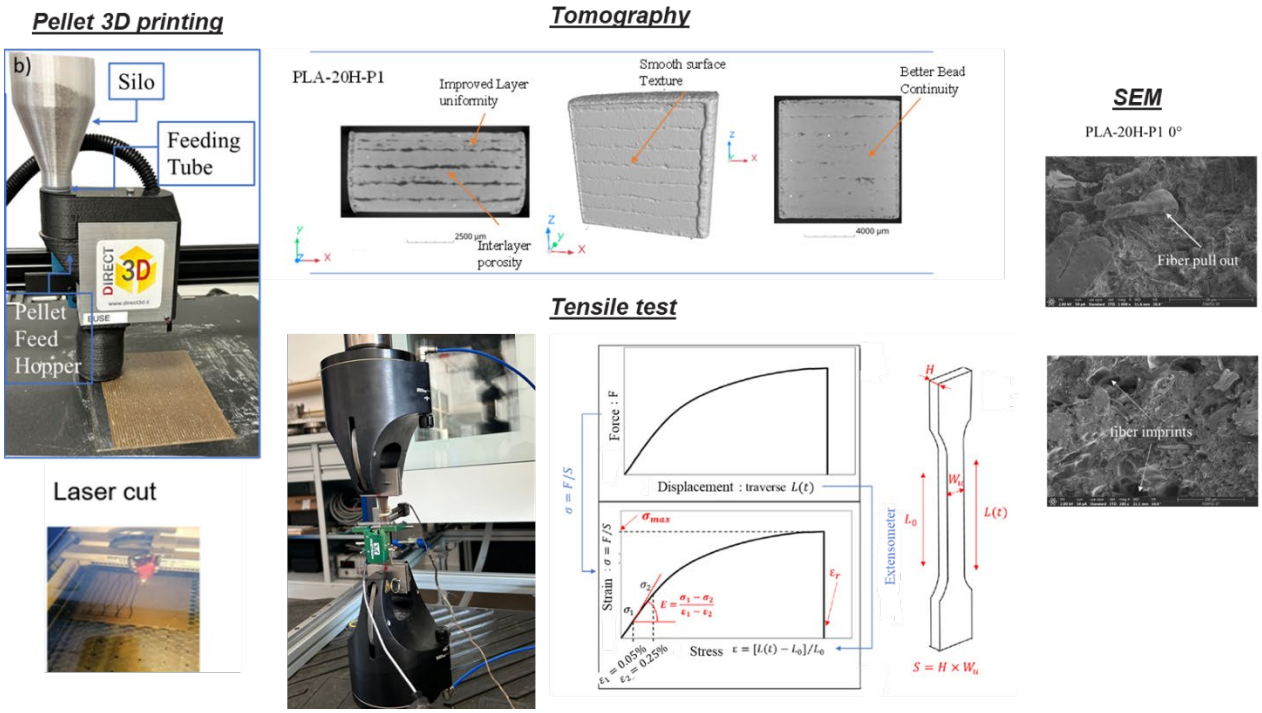

Fig. 1. PLA–hemp composite characterization. Left: Pellet-based 3D-printing (P-MEX) and laser cutting of ISO 527-4 specimens. Center top: X-ray tomography showing layer uniformity and bead continuity. Center bottom: Tensile testing setup and stress–strain derivation. Right: SEM micrographs of fiber pull-out and imprints used for porosity modeling. , adapted from [1].

Microstructural Analysis

Differential scanning calorimetry (DSC) measurements revealed matrix crystallinity of 52% for pure PLA, reduced to 38% in the fiber-reinforced composite due to heterogeneous nucleation interference from the cellulosic hemp reinforcement, as reported in Table 1. High-resolution X-ray computed tomography (CT) combined with scanning electron microscopy (SEM) quantified porosity

distribution, confirming 8-9% void content primarily manifested as localized inter-bead voids rather than intra-bead defects (Fig.1). Although CT data showed a bimodal fiber orientation peaking at 20°, the composite is modeled as macroscopically isotropic. This is justified by the significant density of fibers distributed between 30° and 90°, which compared to strictly anisotropic histograms suggests a degree of diversity consistent with virtually isotropic behavior[1,7,8]. This is confirmed by the experimental data, where the Poisson's ratio varied only marginally (0.32–0.44) between loading directions. These minimal differences justify using a single average value ($\nu = 0.37$), as the global response is dominated by the matrix and a near-random fiber distribution. Consequently, this compact strategy avoids complex orientation-dependent stress homogenization while accurately capturing the primary viscoelastic-plastic phenomena.

Table 1. Key microstructural and mechanical properties of PLA-hemp composites

Composition	**Porosity [%]**	**DC [%]**	**E [GPa] Print direction**	**σ_u [MPa]**	**ε_u [%]**
Pure PLA	-	52	3.2	Brittle failure	<1
PLA – Hemp - « PEG20k » 5wt% (optimal)	8-9	38	3.6	40	~3

Mechanical Testing

Uniaxial tensile testing followed ISO 527-4 protocol using an MTS Criterion system equipped with a 5 kN load cell and extensometer (gauge length 25 mm). Displacement-controlled monotonic loading at engineering strain rate 0.001 s^{-1} captured characteristic nonlinear stress-strain response: initial linear elastic regime to approximately 0.25% strain followed by viscoplastic upturn culminating in ductile failure near 3% engineering strain. Additional tests spanning strain rates 10^{-3} to 10^{2} s^{-1}confirmed pronounced rate sensitivity, while constant-load creep experiments at stress levels below 35% of ultimate strength demonstrated significant time-dependent deformation accumulation. The plasticizer addition tripled failure ductility relative to unreinforced PLA while controlled porosity levels proved essential reductions below 4% porosity shifted response toward elastic-dominated behavior.

Micromechanical Constitutive Framework

The constitutive description is based on a multiplicative split of the deformation gradient into elastic and viscoelastic-plastic parts,

$$\mathbf{F} = \mathbf{F}^{e}\mathbf{F}^{vep}, \text{ with } \det(\mathbf{F}^{vep}) = 1, \tag{1}$$

so that elastic and time-dependent mechanisms are clearly separated. Short hemp fibers (average length 160 μm) are assumed to be homogeneously and randomly distributed, strongly bonded to the PLA matrix, with low intra-bead porosity (<10%); as a consequence, the initial response is considered macroscopically isotropic and governed by fiber-dominated elasticity. In what follows, the superscripts f, c, a denote fiber, crystalline and amorphous phases, respectively.

The rheological structure corresponds to a three-dimensional extension of the Maxwell model, previously used for glassy polymers and semi-crystalline thermoplastics, here adapted to a three-phase composite (fibers, crystalline regions and amorphous matrix) [9–11].

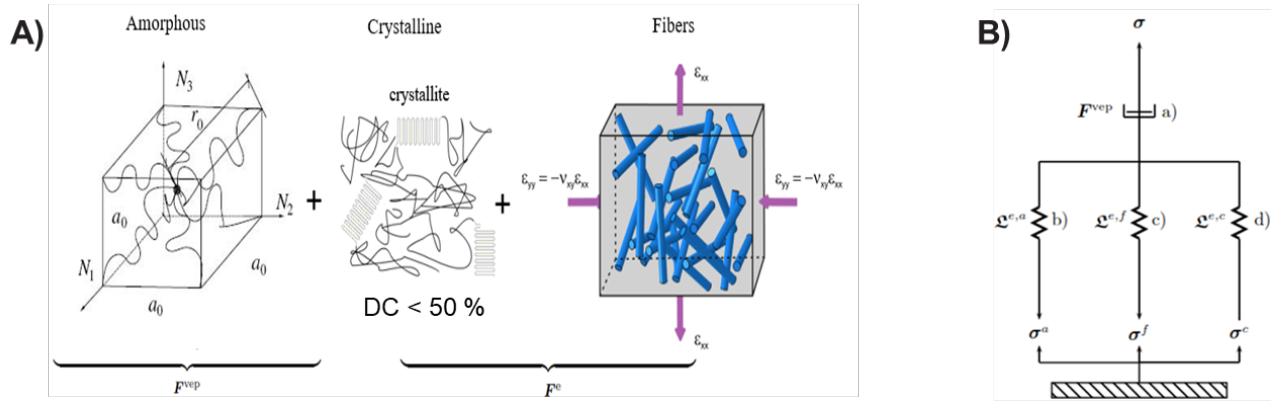

Fig.2. (A) Schematic microstructure of the PLA–hemp composite with amorphous, crystalline and fiber phases contributing respectively to viscoelastic-plastic and elastic deformation. (B) Equivalent Maxwell-type rheological model where the amorphous phase is modeled by a nonlinear dashpot in series with elastic springs representing amorphous, crystalline and fiber phases, adapted from [1].

Elastic response of the phases

The elastic behaviour of each phase is described using a Hencky-type law. For the fiber phase, the macroscopic stress reads

$$\boldsymbol{\sigma}^{f} = \xi\, \boldsymbol{\mathcal{L}}^{e,f} : \ln \mathbf{v}^{e} = \xi E^{f}/(1+\nu^{f}) \ln \mathbf{v}^{e} + \xi E^{f}/\left[3\left(1-2\nu^{f}\right)\right] \mathrm{tr}\,(\ln \mathbf{v}^{e})\mathrm{i}, \tag{2}$$

Where ξ is the fiber content, and E^{f}, ν^{f} are the fiber Young's modulus and Poisson's ratio, and $\boldsymbol{\mathcal{L}}^{e,f}$ is the corresponding elastic stiffness tensor [9]. The crystalline regions are treated in the same way,

$$\boldsymbol{\sigma}^{c} = (1-\xi)\, \boldsymbol{\mathcal{L}}^{e,c} : \ln \mathbf{v}^{e} = (1-\xi)E^{c}/(1+\nu^{c}) \ln \mathbf{v}^{e} + (1-\xi)E^{c}/[3(1-2\nu^{c})] \mathrm{tr}\,(\ln \mathbf{v}^{e})\mathrm{i}, \tag{3}$$

with E^{c}, ν^{c} the crystalline modulus and Poisson's ratio. The moduli of the amorphous phase and fibers are obtained from simple mixing relations,

$$(1-\zeta)E^{m} = \chi E^{c} + (1-\chi)(1-\zeta)E^{a}, \quad E = \xi E^{f} + (1-\xi)(1-\zeta)E^{m} \tag{4, 5}$$

linking the measured composite modulus E, matrix modulus $\mathbf{E^{m}}$, porosity $\boldsymbol{\zeta}$ and crystallinity χ. The amorphous phase is also modeled as Hencky-elastic,

$$\boldsymbol{\sigma}^{a} = (1-\xi)\, \boldsymbol{\mathcal{L}}^{e,a} : \ln \mathbf{v}^{e} = (1-\xi)E^{a}/(1+\nu^{a}) \ln v^{e} + (1-\xi)E^{a}/[3(1-2\nu^{a})] \mathrm{tr}\,(\ln \mathbf{v}^{e})\, \mathbf{i} \tag{6}$$

and the total stress is the sum of the phase contribution.

Viscoelastic-plastic deformation

Time-dependent deformation is assumed to occur only in the amorphous phase. For brevity, only uniaxial-type loading is discussed here, but the model is fully three-dimensional. The viscoelastic-plastic rate of deformation is defined as

$$\bar{\mathbf{D}}^{vep} = \left(\frac{\dot{\gamma}^{vep}}{2\tau} - \frac{1}{\eta}\right) \boldsymbol{\tau}^{dev}, \tag{7}$$

with $\tau = \sqrt{1/2 \mathrm{tr}\,(\boldsymbol{\sigma}^{dev})^{2}}$ and the plastic multiplier

$$\dot{\gamma}^{vep} = \dot{\gamma}_{0}^{a} \left(\frac{\tau}{s^{a} - 1/3\beta I_{1}}\right)^{1/m} \geq 0, \tag{8}$$

where $\dot{\gamma}_{0}^{a}$, m (the limit $m \to 0$ corresponds to the rate-independent limit), and β denote the material parameters, s^{a} is an internal state variable (representing the molecular resistance to plastic shear flow

[12] and $I_1 = \mathrm{tr}(\boldsymbol{\sigma})$ is the first invariant of the stress indicating pressure: plastic deformation is suppressed under compression, that is, micro-cracks are opened in tension and partially closed in compression. This formulation, corresponding to a three-dimensional Maxwell-type rheology, allows one to capture nonlinear monotonic loading, stress relaxation, creep under low stresses and residual strains upon unloading with a compact set of parameters.

Parameter Identification and Model Validation

The parameters of the elastic part of the model were obtained from the initial slopes of the experimental stress–strain curves of the composite, the PLA matrix and an amorphous PLA reference. The Young's modulus of the composite in the printing direction was extracted from the linear regime up to a strain of 0.25%, and the corresponding values for the matrix and amorphous phase were obtained from printed and extruded specimens, respectively. The moduli of the crystalline and fiber phases were then computed using the mixing relations in Eqs. (4,5), while a common Poisson's ratio was adopted based on the measured near-isotropic response.

The viscoelastic–plastic parameters shown in Table 2 were identified by fitting the monotonic tensile curves at room temperature, with σ_0 chosen to match the onset of nonlinearity and the remaining parameters tuned to reproduce the shape of the loading and unloading branches. The calibrated model accurately captures the measured stress–strain response up to failure in both the printing and transverse directions, with errors in elastic modulus and ultimate strength within the experimental scatter. This agreement justifies the use of the compact phase description and the localisation of time-dependent deformation in the amorphous phase.

Table 2. Calibrated constitutive parameters [1].

Symbol	Description	Value [Unit]
E	Composite Young's modulus	3.6 GPa
E^m	PLA matrix modulus	3.2 GPa
E^a	Amorphous PLA modulus	3.0 GPa
ν	Poisson's ratio (all phases)	0.37
β	Pressure sensitivity parameter	0.2
η	Viscosity of the composite	4.0×10^4 MPa·s
m	Rate-sensitivity exponent	0.11
$\dot{\gamma}_0^a$	Reference shear strain rate (prefactor in $\dot{\gamma}^{vep}$).)	4.0×10^{-3} s^{-1}
s^a	Shear resistance to plastic flow	26 MPa

Results and Forming Process Implications

The primary outcome of this study is the validation of a compact micromechanical constitutive law for natural short-fiber reinforced PLA that reproduces elastic–viscoplastic responses with a limited number of parameters. The agreement obtained for stress–strain curves, unloading, creep and stress relaxation indicates that the simplifying assumptions (random short fibers, suppressed lattice anisotropy, viscoelastic–plastic flow confined to the amorphous phase) are sufficient for the forming-relevant strain range considered here ($\varepsilon < 10\%$).

Model validation confirms accurate capture of the measured mechanical properties: the composite elastic modulus is approximately E =3.6 GPa, the ultimate tensile strength about 40 MPa and the failure strain close to 3%, with faithful reproduction of unloading hysteresis and stress-relaxation transients. Rate-dependent predictions align with experiments across several orders of magnitude in strain rate, while creep accumulation at 20% of the ultimate strength matches experimental observations over extended hold times. The framework generalises robustly to engineering strains below 10%, which encompasses typical conditions in cold-forming and incremental forming of such biocomposites.

Fig. 3 illustrates predicted creep-strain evolution at 20% of the ultimate stress for different porosity levels, highlighting an optimal ductility window at 8–9% controlled porosity. Porosity reductions to 4% shift the response to elastic-dominated.

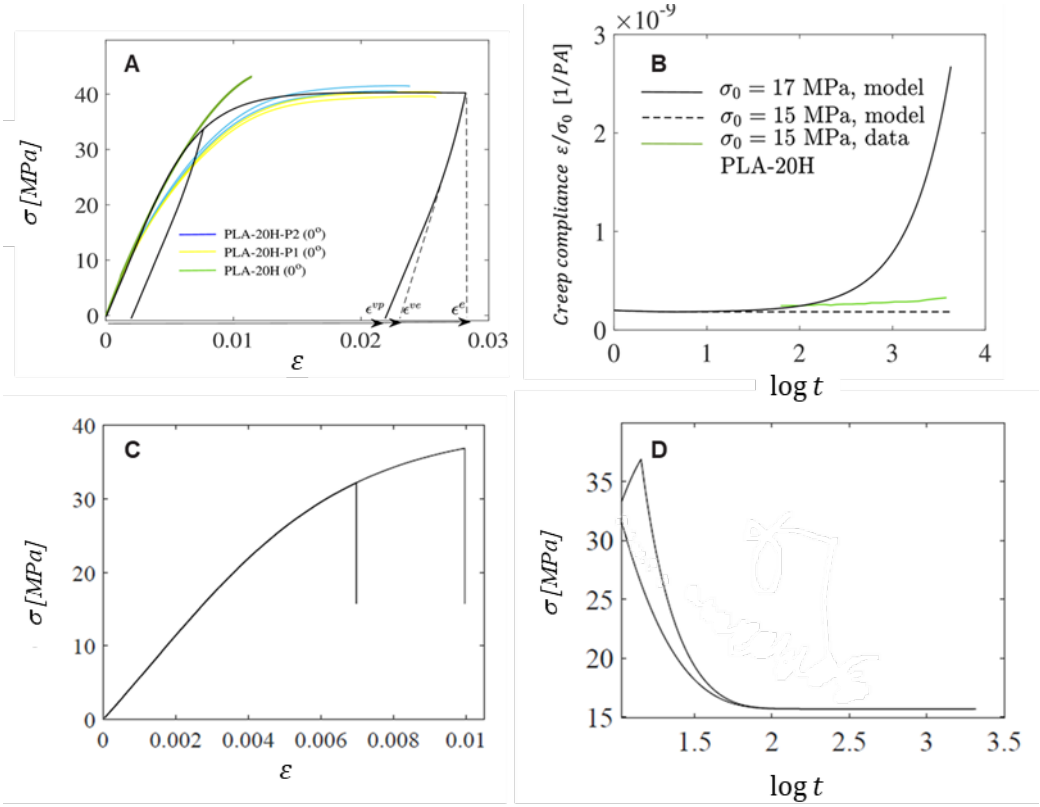

Fig.3. Mechanical response of PLA–hemp composites. (A) Tensile stress–strain curves for PLA-20H and plasticized variants (P1, P2), with illustration of elastic, viscoelastic, and viscoplastic strain components. (B) Predicted vs. experimental creep compliance (ε/σ_0) over one hour at $\sigma = \frac{1}{3}\sigma_{UTS}$ (C–D) Predicted stress–strain and log-time relaxation curves showing viscoelastic stress decay, adapted from [1].

From a manufacturing perspective, pellet-based material extrusion (P-MEX) processing enables precise porosity control through layer thickness, print speed and nozzle-temperature settings, providing a practical pathway to tailor ductility and stiffness for near-net-shape component fabrication. When combined with the constitutive model, this offers a physics-based link between process parameters, microstructure and forming performance. The additional use of machine-learning surrogates, trained on synthetic data generated by the model, facilitates rapid virtual screening of compositions and printing conditions and can substantially reduce the need for physical prototype testing in future optimisation studies.

Discussion and Future Developments

The present work demonstrates that a compact micromechanical constitutive model can describe the elastic–viscoplastic behaviour of PLA–hemp biocomposites over the strain and time scales relevant for forming. The good agreement obtained for stress–strain curves, unloading, creep and relaxation confirms that the underlying assumptions, random short fibers, strong fiber–matrix bonding, suppressed lattice-scale anisotropy and viscoelastic–plastic flow confined to the amorphous phase are sufficient within the investigated ranges of global strain ($\varepsilon < 10\%$) and porosity ($\approx$ 8–9%). A small set of parameters identified from uniaxial tensile tests reproduces the main features of the response, including rate effects and residual strains after unloading.

A key advantage of the modelling strategy is that the phase moduli are directly linked to measurable or controllable microstructural quantities such as fiber content, degree of crystallinity and porosity, rather than being purely phenomenological. This provides a physically interpretable connection between processing, microstructure and mechanical behaviour. In particular, the calibrated model captures the experimentally observed trends that increasing porosity enhances deformability but lowers stiffness, while higher fiber content stiffens the composite at the expense of ductility, which is essential for defining forming windows where sufficient plasticity is required without losing the stiffness advantage from reinforcement.

The current formulation is nevertheless subject to several limitations. It is calibrated and validated essentially under uniaxial tension, and the assumption of macroscopic isotropy relies on the fiber orientation distribution induced by pellet-extrusion 3D-printing. Strongly aligned materials or multiaxial forming paths will require an explicit orthotropic extension of the elastic stiffness and possibly of the viscoplastic flow rule. Furthermore, the model is isothermal and does not account for temperature-dependent phenomena such as glass transition, recrystallisation or thermal softening, which can influence warm-forming and high-rate applications. Fatigue and cyclic degradation are not considered either; only monotonic and simple creep/relaxation histories are addressed.

These limitations point to natural directions for future work. On the constitutive side, extensions include introducing temperature dependence into the viscoelastic–plastic part, adding damage or porosity-evolution variables to capture micro-void growth, and incorporating cyclic plasticity mechanisms to predict fatigue life under repeated loading. A more detailed treatment of fiber orientation, for example through orientation tensors or evolution equations, would also broaden the range of forming processes that can be simulated.

As a complementary direction, the validated constitutive model was used as a physics-based data generator for machine-learning approaches [1,13]. By systematically varying porosity (0–15%), fiber content (0–30 wt%) and degree of crystallinity (10–50%), approximately 10^4 synthetic stress–strain and creep curves were produced and used to train Support Vector Regression (SVR) surrogates with radial basis function kernels. The inputs consisted of strain, time and microstructural parameters, and the outputs were the corresponding stresses. The trained surrogates reproduced the constitutive model predictions with coefficients of determination R^2 greater than 0.99 and mean relative errors below 2% on a held-out test set, while reducing the computation time for 1-year creep simulations from the order of 10 h to about 0.1 s. These results are not required for the validation of the constitutive law itself, but they demonstrate how the compact model can underpin future digital-twin and optimisation studies by providing high-quality training data for fast metamodels, as illustrated in Fig. 4.

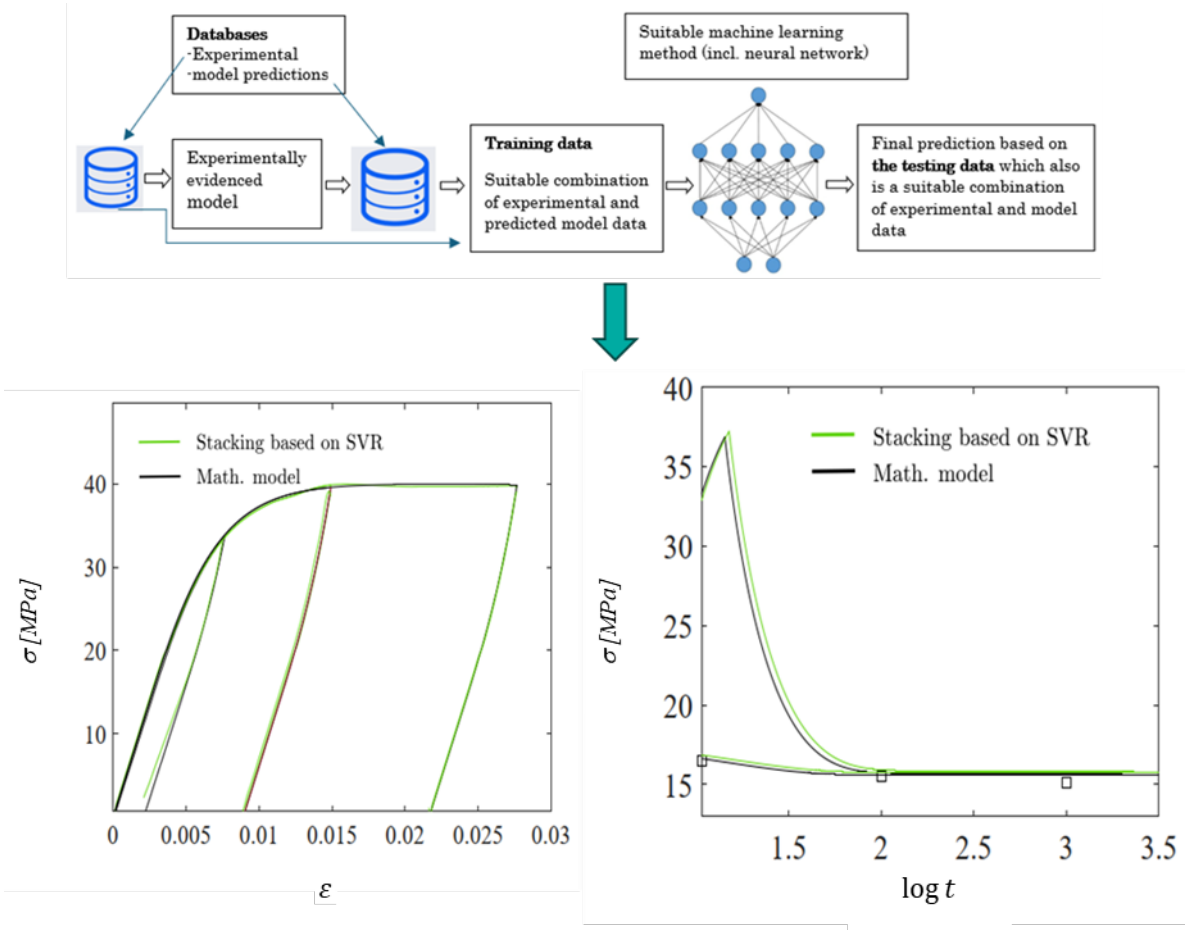

Fig. 4. Machine-learning surrogate based on the constitutive model: left, schematic workflow from experimental and model data to trained SVR; middle, comparison between the SVR surrogate and the constitutive model for a tensile loading–unloading cycle; right, corresponding stress-relaxation response versus log t. The surrogate closely reproduces the physics-based model while being several orders of magnitude faster, adapted from [1].

Summary

A compact micromechanical constitutive model has been developed and validated for predicting the elastic–viscoplastic deformability of PLA–hemp biocomposites over forming-relevant strains and times. The framework links phase properties directly to fiber content, degree of crystallinity and porosity, and reproduces measured stress–strain curves, unloading, creep and stress relaxation for an optimal composition combining 20 wt% hemp reinforcement, 5 wt% PEG plasticisation and 8–9% engineered porosity, which provides thermoplastic-like failure ductility while maintaining competitive stiffness. As a perspective, synthetic datasets generated by the constitutive model have been used to train accurate machine-learning surrogates, demonstrating that substantial speed-ups for long-term simulations can be achieved and opening the way to digital-twin applications for industrial-scale materials optimisation and process design.

References

[1] Niang N, Barriere T, Gabrion X, Holopainen S, Placet V. Predicting the deformability of natural short-fiber reinforced polymer composites through combined constitutive mathematical and AI-based modeling approaches. Composites Science and Technology 2025;273:111353. https://doi.org/10.1016/j.compscitech.2025.111353.

[2] Modniks J, Andersons J. Modeling the non-linear deformation of a short-flax-fiber-reinforced polymer composite by orientation averaging. Composites Part B: Engineering 2013;54:188–93. https://doi.org/10.1016/j.compositesb.2013.04.058.

[3] Qi L, Tian W, Zhou J. Numerical evaluation of effective elastic properties of composites reinforced by spatially randomly distributed short fibers with certain aspect ratio. Composite Structures 2015;131:843–51. https://doi.org/10.1016/j.compstruct.2015.06.045.

[4] Hessman PA, Welschinger F, Hornberger K, Böhlke T. On mean field homogenization schemes for short fiber reinforced composites: Unified formulation, application and benchmark. International Journal of Solids and Structures 2021;230–231:111141. https://doi.org/10.1016/j.ijsolstr.2021.111141.

[5] R.A. Ilyas, S.M. Sapuan, M. M. Harussani, M.Y.A.Y. Hakimi, M.Z.M. Haziq, M.S.N. Atikah, et al. Polylactic Acid (PLA) Biocomposite: Processing, Additive Manufacturing and Advanced Applications. Polymers 2021. https://doi.org/10.3390/polym13081326.

[6] Le Duigou, Masahito Ueda, David Correa, Ryosuke Matsuzaki, Mickaël Castro. A review of 3D and 4D printing of natural fibre biocomposites. Materials & Design 2020. https://doi.org/10.1016/j.matdes.2020.108911.

[7] Mortazavian S, Fatemi A. Effects of fiber orientation and anisotropy on tensile strength and elastic modulus of short fiber reinforced polymer composites. Composites Part B: Engineering 2015; 72: 116–29. https://doi.org/10.1016/j.compositesb.2014.11.041.

[8] Barriere T, Placet V, Holopainen S, Niang N. Predicting the Deformation Behavior of Biocomposites using Combined Mathematical and AI-Based Modeling. Procedia Structural Integrity 2026;80:212–8. https://doi.org/10.1016/j.prostr.2026.02.021.

[9] Belytschko T, Liu WK, Moran B. Nonlinear Finite Elements for Continua and Structures. Chichester: John Wiley & Sons, Ltd; 2000.

[10] Holopainen S, Barriere T. Modeling of mechanical behavior of amorphous solids undergoing fatigue loadings, with application to polymers. Computers & Structures 2018;199:57–73. https://doi.org/10.1016/j.compstruc.2018.01.010.

[11] Barriere T, Gabrion X, Holopainen S. A compact constitutive model to describe the viscoelastic-plastic behaviour of glassy polymers: Comparison with monotonic and cyclic experiments and state-of-the-art models. International Journal of Plasticity 2019;122:31–48. https://doi.org/10.1016/j.ijplas.2019.05.010.

[12] Anand L, Ames NM. On modeling the micro-indentation response of an amorphous polymer. International Journal of Plasticity 2006; 22: 1123–70. https://doi.org/10.1016/j.ijplas.2005.07.006.

[13] Laycock BG, Chan CM, Halley PJ. A review of computational approaches used in the modelling, design, and manufacturing of biodegradable and biobased polymers. Progress in Polymer Science 2024;157:101874. https://doi.org/10.1016/j.progpolymsci.2024.101874.